COMPUTATIONAL INVESTIGATIONS OF CARBONYL REACTIONS: COMPARISON BETWEEN NUCLEOPHILIC ADDITION VERSUS ENOLATE FORMATION IN THE REACTION OF ACETALDEHYDE WITH HYDROXIDE ION

JULIANTO PRANATA

Department of Chemistry and Biochemistry, University of Arkansas, Fayetteville, Arkansas 72701, USA

Reaction pathways leading to nucleophilic addition and enolate formation were investigated for the reaction between acetaldehyde and hydroxide anion. *Ab initio* calculations predict small activation barriers for both reactions in the gas phase. Monte Carlo simulations were performed to assess the effects of aqueous solvation. It was found that both reaction pathways involve significant solvent-induced activation barriers, in addition to effecting some structural changes in the transition state.

INTRODUCTION

Carbonyl compounds occupy an important position in organic chemistry. Many different compounds contain the carbonyl functionality, and their reactions are fundamental to many synthetically useful transformations. Many biologically important molecules are carbonyl compounds, proteins being the most obvious example. Our group is currently involved in the computation of potential energy surfaces for the reactions of carbonyl compounds. Our previous work in this area concerned the base-promoted hydrolysis of esters and amides.[1,2] Similar processes, namely the nucleophilic addition to a carbonyl group, have been examined by many other workers.[3-7] We have also studied other aspects of carbonyl chemistry, including the basicities of carboxylate lone pairs[8,9] and protonation of amides.[10,11]

The primary focus of the work reported here was to compare the two possible pathways for the reaction between hydroxide ion, representing a base and/or nucleophile, and acetaldehyde, a prototypical carbonyl compound. The first involves nucleophilic addition to form a tetrahedral intermediate, a process similar to those investigated previously.[1-7] The second is abstraction of the α-proton of acetaldehyde, leading to enolate formation. Only a few computational investigations of this process have been reported.[12-14] In the one that is particularly relevant to our work,[13] the reaction pathway was constrained to enforce a colinear proton transfer,

making it difficult to evaluate the actual energetics of the reaction.

In our work, we utilized *ab initio* calculations to compute, without constraints, the reaction pathways for both processes in the gas phase.[15-17] Subsequently we performed Monte Carlo simulations to assess solvent effects.[18] This method of combining *ab initio* calculations and Monte Carlo simulations has been used several times in the past for a variety of chemical reactions.[19-21] Our results indicate that both reactions require very little activation energy in the gas phase, but transfer to the solution phase introduces significant solvent-induced activation energy barriers.

EXPERIMENTAL

Ab initio calculations were performed initially at the RHF/6–31+G(d) level. The incorporation of diffuse functions (the '+' in the basis set designation) is known to be particularly important in the calculation of anionic systems.[22] The transition state for both the nucleophilic addition and enolate formation processes were located. The intrinsic reaction coordinate (IRC) method as implemented by Gonzalez and Schlegel[16,17] was used to follow the reaction pathways from each transition state to the reactants and products. A total of 23 structures were computed for the nucleophilic addition pathway; the enolate formation pathway consisted of 31 structures. Additional *ab initio* calculations performed include a reoptimization of the

stationary points at the MP2/6–31+G(d) level, fol-
lowed by single—point calculations using a larger
basis set, 6–311++G(d,p), and higher levels of
electron correlation, up to MP4(SDTQ). The stationary
points were subjected to frequency calculations at the
RHF/6–31+G(d) and MP2/6–31+G(d) level, both in
order to confirm their character and for thermodynamic
analysis.[15] For this purpose, appropriate scaling factors
(0·9135 for RHF and 0·9646 for MP2)[23] [strictly, these
scale factors were developed for the 6–31G(d) basis
set (without the diffuse functions) and only for the
calculation of zero point energies; however, in the
absence of more suitable alternatives we feel their use
in the current context is appropriate] were used on the
computed frequencies, and modes with frequencies less
than 500 cm⁻¹ were treated as classical rotations. The
frequency calculations on the stationery points for the
enolate-forming reaction were also use to calculate
deuterium kinetic isotope effects, the results of which
are presented elsewhere.[24]

Monte Carlo simulations were performed on an
isothermal–isobaric ensemble consisting of the reacting
system plus 263 water molecules in a cubic box with
dimensions ca $20 \times 20 \times 20$ Å^3. Periodic boundary
conditions were employed. The TIP4P model for water[25]
and standard OPLS Lennard–Jones parameters[26] for the
solute were utilized. Partial atomic charges were
obtained by fitting to ab $initio$-derived electrostatic
potentials[27] for all the structures computed along the
reaction pathways. These options have been shown to
produce reasonably accurate free energies of hydra-
tion.[28] A series of simulations incorporating statistical
perturbation theory[18] were utilized to compute the
changes in the free energies of hydration along the
reaction pathway. In most cases one or two simulations
are sufficient to connect any two neighboring points
along the pathway. Each simulation consists of the
generation 10^6 configurations for equilibration, followed
by 2×10^6 configurations for averaging.

Ab $inito$ calculations were performed using the
Gaussian-92 program[29] on a Silicon Graphics Indigo R-
4000 computer. Monte Carlo simulations were per-
formed   using   the   BOSS   program[30]   on   a
Hewlett–Packard Apollo Series 700 computer.

RESULTS AND DISCUSSION

Gas-phase reaction pathways

Optimized structures for the reactants, transition states
and products for both nucleophilic addition and enolate
formation processes are displayed in Figure 1, with the
bond distances listed in Table 1. Energy related results
are listed in Table 2. The energy profiles are shown in
Figures 2 and 3. It was found that following the IRC
pathway from either transition state resulted in identical
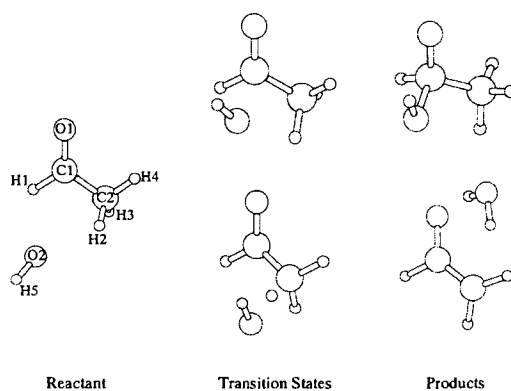structures for the reactants.

Figure 1. Structures of the reactants, transition state and
products for the nucleophilic addition (top) and enolate
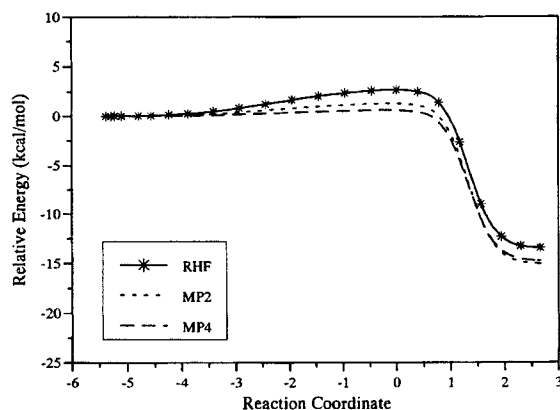formation (bottom) pathways

Figure 2. Gas-phase electronic energy profile for the nucleophilic
addition reaction. For this and Figure 3, the RHF profile was
explicitly calculated using IRC computations and the MP2 and
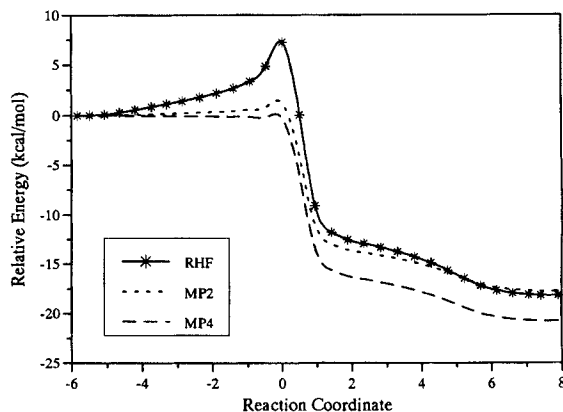MP4 profiles were interpolated from the stationary points

Figure 3. Gas-phase electronic energy profile for the enolate
formation reaction. See caption to Figure 2

Table 1. Optimized bond distances (Å)[a]

Bond	Reactant	Nucleophilic TS	Nucleophilic product	Enolate TS	Enolate product
C1—O1	1·2054	1·2074	1·3064	1·2118	1·2613
	1·2410	1·2405	1·3234	1·2458	1·2954
C1—H1	1·0869	1·0833	1·1100	1·1011	1·1016
	1·1011	1·0969	1·1219	1·1130	1·1143
C1—C2	1·5019	1·5055	1·5393	1·4507	1·3688
	1·4980	1·5040	1·5368	1·4545	1·3812
C2—H2	1·0826	1·0790	1·0912	1·3014	
	1·0978	1·0938	1·0989	1·2212	
C2—H3	1·0873	1·0940	1·0891	1·0885	1·0781
	1·0976	1·1002	1·0974	1·0957	1·0877
C2—H4	1·0864	1·0826	1·0877	1·0863	1·0793
	1·0950	1·0945	1·0956	1·0936	1·0884
C2—O2	2·9084	2·3680	1·4684		
	2·8885	2·4787	1·5255		
H2—O2	2·4654			1·3521	0·9473
	2·1505			1·5181	0·9722
O2—H5	0·9495	0·9499	0·9482	0·9500	0·9700
	0·9763	0·9770	0·9781	0·9762	1·0016
O1—H5					1·8228
					1·7711

[a]The two values shown for each parameter are optimized at RHF/6–31+G(d) and MP2/6–31+G(d), respectively.

Table 2. Energy-related quantities from *ab initio* calculations[a]

	Reactant	Nucleophilic TS	Nucleophilic product	Enolate TS	Enolate product
RHF/6–31+G(d)	−228·327402	2·7	−13·4	7·3	−18·1
MP2/6–31+G(d)	−228·978059	1·3	−15·0	1·2	−17·7
RHF/6–311++G(d,p)	−228·392877	2·7	−11·6	5·3	−20·4
MP2/6–311++G(d,p)	−229·120736	1·2	−15·0	−0·6	−22·0
MP3/6–311++G(d,p)	−229·125049	1·6	−17·3	0·6	−24·1
MP4(DQ)/6–311++G(d,p)	−229·133889	1·8	−15·5	1·4	−21·5
MP4(SDQ)/6–311++G(d,p)	−229·146190	1·3	−14·7	1·0	−20·5
MP4(SDTQ)/6–311++G(d,p)	−229·176896	0·6	−14·7	−0·3	−20·7
E_{vib}^{298}[RHF/6–31+G(d)]	42·7	42·9	44·9	39·7	43·3
S^{298}[RHF/6–31+G(d)]	82·2	73·6	68·5	75·4	79·8
E_{vib}^{298}[MP2/6–31+G(d)]	42·7	42·6	44·6	40·3	43·1
S^{298}[MP2/6–31+G(d)]	79·8	74·0	68·8	75·5	77·5
ΔG^{298}		2·2	−9·6	−1·5	−19·7

[a]Electronic energies of transition states and products are in kcal mol^{-1} relative to the reactant, whose energy is shown in atomic units. Vibrational energies are in kcal mol^{-1}; they include zero-point energies plus additional terms due to population of higher vibrational levels. Entropies are in cal mol^{-1}K^{-1}. ΔG^{298} are in kcal mol^{-1} relative to the reactant; the values shown incorporate the MP4(SDTQ) electronic energies and MP2-derived vibrational energies and entropies.

Optimizations at RHF and MP2 levels [both with the 6–31+G(d) basis set] result in similar geometries for transition states and minima. As expected, in general MP2 bond distances are somewhat longer.[31,32] A notable exception is the C1—C2 distance, which is sometimes shorter at the MP2 level. In addition, non-bonded distances in the reactant complex and the enolate product complex are shorter at the MP2 level, suggesting tighter

complexes. In the transition state for enolate formation, comparison of the C2—H2 and H2—O2 distances suggests an earlier transition state at the MP2 level.

It is worth noting that transition states can actually be found for both processes. Many previous calculations on nucleophilic additions to carbonyl compounds concluded that there is no barrier to the formation of the tetrahedral intermediate.[3,6] In contrast, we found activation free energy barriers for the hydrolysis of esters and amides,[1,2] and likewise here. The electronic energy contribution to this barrier is small, but entropic contributions make it larger (Table 2). This is expected because a bond is being formed; the entropy is even smaller in the product where the bond is fully formed. In spite of all this, the free energy barrier remains small (about 2 kcal mol^{-1}), probably comparable to the limits of accuracy of the computational model. It is possible that this reaction has a negligible activation energy, but it would not be correct to say that the process is energetically 'downhill all the way.' In fact, the energy profile is fairly flat until just past the transition state, where C—O bond formation is actually occurring. Then, and only then, does the energy start to decrease.

The existence of a barrier is also ambiguous for the enolate formation process. A substantial barrier is found with RHF-level calculations, but inclusion of electron correlation drastically reduces the barrier height. Beyond the MP2 level, the barrier height remains low, at times disappearing altogether. Inclusion of entropic contributions decreases the barrier further. Again, this is expected. The process is a proton transfer, and in the transition state the proton is loosely bound to *both* the hydroxide ion's oxygen and the aldehyde's α-carbon, which restricts its motion and reduces the system entropy. The entropy then increases towards the products, which is a bimolecular complex. Overall, this reaction also has negligible activation free energy in the gas phase. However, like nucleophilic addition, the energy does not start to go down until proton transfer is actually in progress. Once the proton has been transferred, the resulting enolate—water complex is not at a local minimum. Following the IRC pathway, a local minimum is not achieved until the water molecule has moved to the other side of the enolate to form a hydrogen bond with its oxygen atom (Figure 1). This product complex has a lower entropy than the reactants (Table 2), because it is held together by a relatively stronger hydrogen bond, whereas the reactants are at best an ion—dipole complex.

The orientation of the product looks ideal for a reverse proton transfer to form the enol—hydroxide complex. However, numerous attempts to explore this additional pathway were unsuccessful. Coaxing the proton to transfer to the enolate oxygen while moving the hydroxide away resulted in a continuous energy increase, without any sign of a saddle point. It is likely that the enol—hydroxide complex is energetically much less favorable and does not lie in a potential energy well; the enol tautomer of acetaldehyde is certainly

much less stable than the keto form. However, it should be re-emphasized that these calculations refer to gas-phase processes. Solvation will certainly have an effect.

Solvent effects

The gas-phase energy profiles of both reactions indicate substantially exothermic reactions. In aqueous solution, a substantial reduction or even reversal of this exothermicity may be expected. The reactant complex includes a hydroxide ion, a fairly 'hard' base that is expected to be well solvated. The products are either a tetrahedral intermediate or an enolate, both of which have much more diffuse charge distributions and thus expected to benefit less from solvation. It may also be expected that the enolate has the more diffuse charge distribution because of resonance delocalization.

These expectations are generally confirmed by the results of the Monte Carlo simulations. In Figures 4 and 5, the relative free energy of solvation is plotted as a
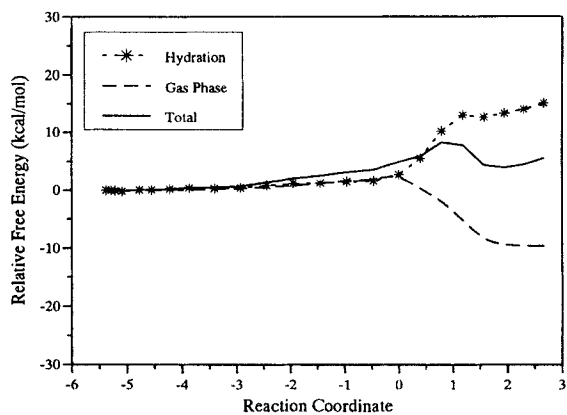
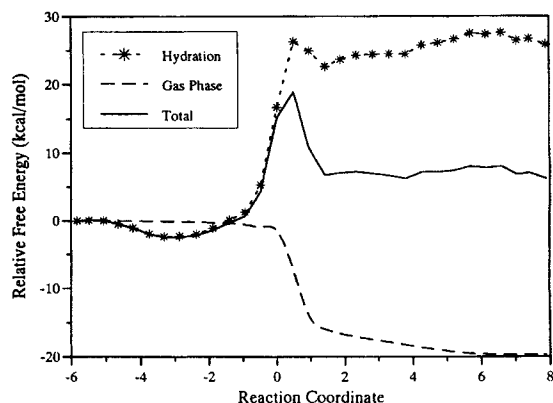Figure 4. Free energy profiles for the nucleophilic addition reaction

Figure 5. Free energy profiles for the enolate formation reaction

function of the reaction coordinate for both processes. The figures also show the gas-phase free energy profile, interpolated from the *ab initio* data, and the total free energy profile obtained as the sum of the gas-phase and hydration free energy contributions. The solvation free energy profiles indicate that the most significant change occurs over a relatively narrow range of the reaction coordinate, corresponding to the region where the gas-phase energy is also changing the most rapidly. This is the region where the actual bond-making and -breaking process takes place.

The calculated solvent effects are summarized in Table 3. For both reactions the solvent effect is significant. Solvent-induced activation barriers are observed. In addition, the reactions, which are significantly exothermic in the gas phase, become endothermic, owing to the lesser stabilization of the products due to the solvent.

In addition to the dramatic changes in the reaction energetics, solvation also causes some structural changes in the stationary points. The transition states of both reactions are slightly shifted towards the products, while the locations of both reactant and product complexes are shifted inward. In other words, all the complexes are tighter in solution. One noticeable aspect of the enolate-forming reaction is that one of the product molecules is water, and in the gas-phase pathway this product water molecule reorients itself until it is hydrogen bonded to the carbonyl oxygen. In aqueous solution, this is of course unnecessary, and the free energy profile in Figure 5 reflects this. The total free energy profile is fairly flat past 1·4 on the reaction coordinate, where the motion is primarily the reorientation of the product water molecule.

It should be noted that the computational procedure employed here does not include a reoptimization of the reacting system's geometry in the solution phase, so the only solvent-induced structural changes detected are shifts along the one-dimensional reaction coordinate. This methodology would *underestimate* the solvent effects, so the actual effect would be even more dramatic.

Some tabulated values for the activation energies for proton transfer reactions in water are in the range of $14-23$ kcal mol^{-1} with activation entropies of -16 to -26 cal mol^{-1} K^{-1},[33] giving free energies of activation in the range $21-29$ kcal mol^{-1}; these are for proton transfers from a variety of organic acids to water. For the enolate formation reaction we studied, the acceptor is hydroxide instead of water, but the calculated free energy of activation in water ($21·4$ kcal mol^{-1}) is consistent with this range.

In the real world, neither the enolate nor the tetrahedral intermediate is a particularly stable structure, and the actual reaction between acetaldehyde and hydroxide ion would probably be an aldol condensation. Thus, both enolate formation and nucleophilic addition would be happening, although in the latter the nucleophile involved would be the enolate, not hydroxide.

CONCLUSIONS

Reaction pathways for the nucleophilic addition and enolate formation in acetaldehyde have been investigated using a combination of *ab initio* calculations and Monte Carlo simulations. Both reactions were found to be substantially exothermic and require very little activation energy in the gas phase. Aqueous solvation has the effect of reversing the exothermicity of the reactions, introducing significant activation energy barriers, and causing some structural changes in the reactants products and transition states for the reactions.

Table 3. Summary of solvent effects

	Reactant	TS	Product
Nucleophilic addition			
Gas phase:			
Position[a]	−5·4	0	2·7
Relative Energy[b]	0	2·2	−9·6
Aqueous phase:			
Position[a]	−5·1	0·8	1·9
Relative free energy[b]	−0·1	8·3	3·9
Enolate formation			
Gas phase:			
Position[a]	−5·8	0	7·9
Relative Energy[b]	0	−1·5	−19·7
Aqueous phase:			
Position[a]	−3·3	0·5	1·4
Relative free energy[b]	−2·5	18·9	6·7

[a] Position along the reaction coordinate as illustrated in Figures 4 and 5.
[b] In kcal mol^{-1}.

REFERENCES

1. J. Pranata, *J. Phys. Chem.* **98**, 1180–1184 (1994).
2. J. F. O'Brien and J. Pranata, *J. Phys. Chem.* **99**, 12759–12763 (1995).
3. S. J. Weiner, U. C. Singh and P. A. Kollman, *J. Am. Chem. Soc.* **107**, 2219–29 (1985).
4. J. D. Madura and W. L. Jorgensen, *J. Am. Chem. Soc.* **108**, 2517–2527 (1986).
5. J. F. Blake and W. L. Jorgensen, *J. Am. Chem. Soc.* **109**, 3856–3861 (1987).
6. J. P.Krug, P. L. A. Popelier and R. W. F. Bader, *J. Phys. Chem.* **96**, 7604–7616 (1992).

7. J. S. Francisco and I. H. Williams, *J. Am. Chem. Soc.* **115**, 3746–3751 (1993).
8. J. Pranata, *J. Comput. Chem.* **14**, 685–690 (1993).
9. A. Kamitakahara and J. Pranata, *Bioorg. Chem.* **23**, 256–262 (1995).
10. J. Pranata and G. D. Davis, *J. Phys. Chem.* **99**, 14340–14346 (1995).
11. A. Kamitakahara and J. Pranata, unpublished results.
12. O. N. Ventura, A. Lledós, R. Bonaccorsi, J. Bertrán and J. Tomasi, *Theor. Chim. Acta* **72**, 175–195 (1987).
13. T. Niiya, M. Yukawa, H. Morishita and Y. Goto, *Chem. Pharm. Bull.* **35**, 4395–4404 (1987).
14. T. Niiya, M. Yukawa, H. Morishita, H. Ikeda and Y. Goto, *Chem. Pharm. Bull.* **39**, 2475–2482 (1991).
15. W. J. Hehre, L. Radom, P. v. R. Schleyer and J. A. Pople, *Ab Initio Molecular Orbital Theory.* Wiley, New York (1986).
16. C. Gonzalez and H. B. Schlegel, *J. Chem. Phys.* **90**, 2154–2161 (1989).
17. C. Gonzalez and H. B. Schlegel, *J. Phys. Chem.* **94**, 5523–5527 (1990).
18. W. L. Jorgensen, *Acc. Chem. Res.* **22**, 184–189 (1989).
19. J. F. Blake and W. L. Jorgensen, *J. Am. Chem. Soc.* **113**, 7430–7432 (1991).
20. D. L. Severance and W. L. Jorgensen, *J. Am. Chem. Soc.* **114**, 10966–10968 (1992).
21. D. K. Jones-Hertzog and W. L. Jorgensen, *J. Am. Chem. Soc.* **117**, 9077–9078 (1995).
22. T. Clark, J. Chandrasekhar, G. W. Spitznagel and P. v. R. Schleyer, *J. Comput. Chem.* **4**, 294–301 (1983).
23. J. A. Pople, A. P. Scott, M. W. Wong and L. Radom, *Is. J. Chem.* **33**, 345–350 (1993).
24. W. C. Alston, II, K. Haley, R. Kanski, C. J. Murray and J. Pranata, *J. Am. Chem. Soc.* **118**, 6562–6569 (1996).
25. W. L. Jorgensen, J. Chandrasekhar, J. D. Madura, R. D. Impey and M. L. Klein, *J. Chem. Phys.* **79**, 926–935 (1983).
26. W. L. Jorgensen and J. Tirado-Rives, *J. Am. Chem. Soc.* **110**, 1657–1666 (1988).
27. C. M. Brenneman and K. B. Wiberg, *J. Comput. Chem.* **11**, 361–373 (1990).
28. H. A. Carlson, T. B. Nguyen, M. Orozco and W. L. Jorgensen, *J. Comput. Chem.* **14**, 1240–1249 (1993).
29. M J. Frisch, G. W. Trucks, M. Head-Gordon, P. M. W. Gill, M. W. Wong, J. B. Foresman, B. G. Johnson, H. B. Schlegel, M. A. Robb, E. S. Replogle, R. Gomperts, J. L. Andres, K. Raghavachari, J. S. Binkley, C. Gonzalez, R. L. Martin, D. J. Fox, D. J. DeFrees, J. Baker, J. J. P. Stewart, and J. A. Pople, *Gaussian 92, Revision B.* Gaussian, Inc., Pittsburgh, PA (1992).
30. W. L. Jorgensen, *BOSS Version 3.1.* Yale University, New Haven, CT (1991).
31. R. F. Frey, J. Coffin, S. Q. Newton, V. Ramek, V. K. W. Cheng, F. A. Momany and L. Schäfer, *J. Am. Chem. Soc.* **114**, 5369–5377.
32. M. Cao, S. Q. Newton, J. Pranata and L. Schäfer, *J. Mol. Struct. (THEOCHEM)* **332**, 251–267 (1995).
33. J. W. Moore and R. G. Pearson, *Kinetics and Mechanisms*, 3rd edn, p. 256. Wiley, New York (1981).